Ultrasonics - Sonochemistry 68 (2020) 105227

Contents lists available at ScienceDirect

Ultrasonics - Sonochemistry

journal homepage: www.elsevier.com/locate/ultson

Ultrasound-assisted intensified crystallization of L-glutamic acid: Crystal nucleation and polymorph transformation

Chen Fang[a,b], Weiwei Tang[a,b], Songgu Wu[a,b], Jingkang Wang[a,b], Zhenguo Gao[a,b,*,2], Junbo Gong[a,b,*,1]

[a] School of Chemical Engineering and Technology, State Key Laboratory of Chemical Engineering, Tianjin University, Tianjin 300072, China
[b] The Co-Innovation Center of Chemistry and Chemical Engineering of Tianjin, Tianjin 300072, China

ARTICLE INFO

Keywords:
Ultrasound
L-glutamic acid
Nucleation
Polymorphic transformation

ABSTRACT

In this paper, the crystallization of L-glutamic acid with application of ultrasound was explored in detail, including the process of nucleation, polymorphic control and polymorphic transformation. The induction time and metastable zone widths (MSZWs) were measured with and without ultrasound during the nucleation process. The induction time and MSZWs were decreased by ultrasound and the induction time was further decreased by higher ultrasonic power. The calculated nucleation parameters (such as interfacial energy, critical nucleus size and critical Gibbs energy) showed an obvious decrease in the presence of ultrasound, indicating that the nucleation was enhanced with application of ultrasound. By adjusting the ultrasonic power in the quench cooling process, the difference in nucleation temperatures would determine the distribution of polymorphs. In further, the polymorphic transformation was investigated quantitatively, and to the best of our knowledge, it was the first time to study the transformation kinetics with ultrasound using Avrami-Erofeev model. In the transformation process, the crystallization mechanism of the stable form was modified by ultrasound. The ultrasound eliminated the nucleation element in the rate-limiting step and facilitated the crystal growth of stable form. Thus, the ultrasound has a profound influence on L-glutamic acid crystallization.

1. Introduction

Solution crystallization is an important and energy-efficient separation process for crystalline material production as well as high value-added properties engineering, which is widely used in the pharmaceutical industry. The properties of the crystals, *e.g.*, purity, stability, crystal size, crystal size distribution (CSD), crystal morphology would determine the value or the function of the crystal products. For pharmaceuticals, the crystal properties have a direct effect on stability, dissolution rate [1], solubility [2] and tableting properties [3], etc. More importantly, the polymorphism phenomenon in crystallization, which is the same component crystals exhibit more than one crystal lattice structure, has a significant effect on drug efficacy or toxicity [4–6]. Thus, numerous researches studied the crystallization process parameters and control recipes to improve product quality and process robustness [7–9]. In the past few years, several external fields were introduced to optimize the crystal product [10–12], in which the ultrasonic irradiation was proved to be one of the most effective technologies to tune crystal properties and intensify the crystallization process [13,14].

The ultrasound devices with the frequencies ranged from 20 kHz up to several gigahertz could form acoustic cavitation in liquid, resulting in the initiation and enhancement of crystallization in a supersaturated solution [15,16]. The application of ultrasound in a crystallization process, or called sonocrystallization, could modify the crystal morphology [17,18], change the crystal size and CSD [19,20], control polymorph formation [21,22], affect crystal agglomeration [23] and enhance process robustness [24]. To evaluate the influence of ultrasound on the nucleation process, the metastable zone widths (MSZWs) which are defined as the region between the solubility curve and the supersolubility curve, and the induction time are widely studied. Zeng et al. [25] reported that the induction time of sodium sulfate was shortened by implementing ultrasound in a cooling crystallization process. Jiang [26] studied the effect of ultrasound on the MSZWs in the

* Corresponding authors at: School of Chemical Engineering and Technology, State Key Laboratory of Chemical Engineering, Tianjin University, Tianjin 300072, China.
E-mail addresses: zhenguogao@tju.edu.cn (Z. Gao), junbo_gong@tju.edu.cn (J. Gong).
[1] ORCID: 0000-0002-3376-3296.
[2] ORCID: 0000-0002-5953-1514.

https://doi.org/10.1016/j.ultsonch.2020.105227
Received 29 November 2019; Received in revised form 9 June 2020; Accepted 10 June 2020
Available online 16 June 2020
1350-4177/ © 2020 Elsevier B.V. All rights reserved.

crystallization of L-glutamic acid and calculated the nucleation parameters (nucleation order and nucleation constant) with Nývlt's model. In further, Mastan et al. [27] calculated theoretical nucleation parameters, *e.g.*, the apparent nucleation order and nucleation rate constant, by combining the experimental MSZWs data with four different nucleation models. For the polymorphic crystallization system, the ultrasonic irradiation could selectively promote the nucleation of a specific crystal form [13,22,28]. What's more, in the system with polymorphic transformation phenomenon, ultrasonic irradiation could accelerate the transformation process to reach steady state, but research remains on the discovery and description of experimental phenomenon [29,30]. Though the ultrasound could be an effective process intensification technology for crystallization, no reported study has focused on the polymorphic transformation kinetics in the presence of ultrasound so far.

L-glutamic acid (LGA) is one of the most important amino acids which plays an active role in treating ulcers, hypoglycemia, epilepsy, Parkinson's and other neurological disorders [31]. The LGA has two crystal polymorphs, metastable α form and stable β form which are prismatic and needle-like, respectively [32–34]. The stable β form crystals are fine and fragile, which can cause difficulties during the filtration and drying processes. Thus, the prismatic α form crystals are usually preferred for downstream processing [35]. Generally, it is difficult to control spontaneous nucleation due to the formation of polymorphic mixture. Hatakka [36] designed a method of reactive crystallization to produce pure α form crystals with application of ultrasound and pointed out that only in high supersaturation (1 M) with ultrasound the pure α form could be obtained. However, some studies also declared that the temperature and solution concentration played a significant role in LGA polymorphs [37–39]. In the current study, a strategy of LGA polymorphic control dependent on the nucleation temperature and solution concentration was proposed with different ultrasonic power in cooling crystallization process.

Hence, in this work, a systematic study of LGA sonocrystallization was investigated, including crystal nucleation, polymorphic control and transformation process. The effect of ultrasound on induction time, MSZWs and nucleation parameters were studied. Besides, the polymorph distribution in the nucleation stage was controlled by changing operation parameters (ultrasonic power and solution concentration). Finally, the solvent-mediated polymorphic transformation was explored with different ultrasonic power. It was the first time to study the transformation process with LGA system in the presence of ultrasound and establish the relationships between transformation kinetic parameters and ultrasonic power. More importantly, the mechanism of each process in the LGA sonocrystallization was discussed in detail.

2. Materials and methods

2.1. Materials

The L-glutamic acid was purchased from J&K Chemical Ltd. (Shanghai, China). The raw material is β form with the purity of 99% (HPLC). Deionized water was prepared by an ultrapure water system (YPYD Co., China) in the laboratory. The deionized water was used as solvent in the following sections: 2.3–2.6.

2.2. Ultrasonic processor

The ultrasonic irradiation frequency was fixed at 20 kHz using an ultrasonic processor (JY92-IIDN, Scientz, China) with the tip diameter of 6 mm providing a maximum irradiation power of 90 W. For all the set of experiments, continuous (100% duty cycle) and pulsed ultrasound were employed in the solutions. The operating parameters used in the experiments were listed in Table S1 and further described in the following sections: 2.3–2.6.

2.3. Induction time measurements

Based on the reported solubility data [37], LGA saturated aqueous solutions were prepared at different temperatures ranging from 308.65 K to 323.15 K, producing supersaturation ratio S of 1.8–3.0 accordingly, in which $S = c/c^*$ (c^* is the saturated concentration at 293.15 K). The solution concentrations that correspond to each supersaturation were shown in Table S2. The solution was mixed homogeneously by magnetic stirrer (ZNCL-BS, Xingke Sci. Ltd., China) at 200 rpm. After stirred for one hour, the solution was filtered via a polytetrafluoroethylene (PTFE) filter with 0.22 μm pores into the vials (~10 mL). Then transferring the vials to a thermostatic water bath (CF41, Julabo, Germany) of 293.15 K rapidly for nucleation experiment at an agitation rate of 200 rpm. And at the same time, the ultrasound was applied in the working solution (~10 mL) with two methods (continuous irradiation and pulsed irradiation) till the detection of nucleation. A series of ultrasonic power (9.0–22.5 W) was applied during continuous irradiation process. In addition, a fixed power of 13.5 W was applied during pulsed irradiation experimental process with duty cycles of 16.7% (10 s ON and 50 s OFF), 50% (30 s ON and 30 s OFF) and 83.3% (50 s ON and 10 s OFF), respectively. Based on the pre-experiments, the choice of ultrasound power should consider the existence of measuring error to make sure that the induction time was large enough to be measured exactly. The occurrence of crystals was detected by visual observation. The induction time (t_{ind}) was the time period between reaching certain supersaturation level and appearing crystals [40]. To compare with the results in continuous irradiation process, the pulsed irradiation experiment was also provided.

2.4. MSZWs measurements

Similarly, based on the reported solubility data [37], 30 mL saturated aqueous solution at different temperatures (348.15 K, 344.15 K, 339.15 K, 334.15 K and 315.15 K) was prepared. The solution concentrations that correspond to each supersaturation were shown in Table S3. Then the saturated solution was preheated to 10 K above the saturated temperature under agitation for 60 min to ensure that the solute was dissolved completely. A turbidity meter (InPro8200, Mettler-Toledo, Switzerland) was used to determine the transparency of the solution. With constant cooling rates (6–90 K/h), nucleation was observed at the moment when a rapid decrease appeared in transparency, and then the temperature was recorded as nucleation temperature. The difference between saturation temperature (T_0) and nucleation temperature (T_1) is the MSZWs (ΔT_{max}/K). The whole cooling process was controlled by a thermostat (Ministat 240, Huber, Germany) with a thermocouple to monitor the temperature. The above experiments were carried out in the absence and presence of ultrasound (continuous irradiation with 22.5 W power) under the agitation rate of 200 rpm to study the influence of ultrasound on MSZWs. The ultrasound was introduced when the solution temperature reached the saturation temperature till the detection of nucleation.

2.5. Ultrasound-assisted polymorphic nucleation

To obtain an obvious distribution of polymorphic nucleation, continuous ultrasound was chosen for this experiment. There were two approaches to investigate the ultrasound-assisted polymorphic nucleation. One approach was to prepare a series of saturated aqueous solution (~30 mL) at different temperatures (348.15 K, 338.15 K, 328.15 K and 313.15 K) in a 100 mL crystallizer, and the solution concentration ranged from 15 mg/mL to 45 mg/mL. The crystallizer was transferred to another thermostatic water bath with setting temperatures (273.15–328.15 K) rapidly for nucleation without any other magnetic agitation. The solution concentrations that correspond to each supersaturation were shown in Table S4. Then 18 W continuous ultrasound was introduced until the solution became slightly turbid. The crystals

were pipetted out immediately and observed by the optical microscope (BX53F, Olympus, Japan) for morphology and polymorph determination. In addition, the experiments without ultrasound were performed for comparison under the same condition. The other approach was to prepare a series of saturated aqueous solutions (~75 mL) within the same concentration range as the first approach. The saturated solution was quickly transferred to the cooling water bath (278.15 K), and the magnetic agitation (200 rpm) was used during the cooling process. Then, a series of continuous ultrasound (7.2–27.0 W) was introduced in the solution until the solution became slightly turbid. Finally, the crystals were observed under the optical microscope to determine the morphology and polymorph, and the experiments without ultrasound were performed for comparison under the same condition.

2.6. Ultrasound-assisted polymorphic transformation

The homogeneous aqueous solution (~75 mL) with the concentration of 45 mg/mL (S = 2.6) was prepared at 353.15 K and then rapidly cooled down to 318.15 K with magnetic agitation of 200 rpm. After stirring the clear solution for about 25 min at 318.15 K, the turbid solution with pure α form crystals was obtained. The concentration of α form crystals in the turbid solution was 23.3 g/kg solvent. Then the turbid solution was stirred (200 rpm) for transformation in the absence and presence of ultrasound at 318.15 K. A series of pulsed irradiation (9.0–27.0 W, duty cycle of 2 s ON and 2 s OFF) was running during the whole transformation process until α form crystals completely transformed to β form crystals. The polymorphic transformation process was monitored by *in-situ* Raman spectroscopy (ReactRaman 785, Mettler-Toledo, Switzerland). Ten samples were pipetted out at certain time intervals during the transformation process and characterized by powder X-ray diffraction (PXRD, Rigaku D/MAX 2500 X-ray diffractometer (Rigaku, Japan) at 40 kV and 100 mA with Cu-Kα radiation (λ = 1.54178 Å)). It should be noted that Raman peaks were more stable in the presence of pulsed ultrasound, and the pulsed ultrasound also reduced the thermal effect, making the results more exact and reliable. Given the above consideration, the pulsed ultrasound was chosen for this experiment.

3. Results and discussion

3.1. Effects of ultrasound on the induction time and MSZWs

The saturated solutions within 314.15–323.15 K temperature scope were quickly cooled to 293.15 K, correspondingly generating supersaturation ratios (2.2–3.0). Fig. 1 reflected the effect of different continuous ultrasonic power (9.0–22.5 W) on the induction time of LGA nucleation, followed by the controlled experiment without ultrasound (named 0 W). Without the ultrasound, a decrease of induction time (from 1270 s to 201 s) was observed with an increase of supersaturation ratio (from 2.2 to 3.0). Besides, the induction time was shortened in the presence of ultrasound and further shortened with the increase of irradiation power at constant supersaturation. Thus, with the highest ultrasonic power (22.5 W), the induction time was the shortest and decreased from 104.5 s to 20 s at the experimental supersaturation ratio scope (2.2–3.0). The decrease of induction time affected by ultrasound was more significant at lower supersaturation compared to that at higher supersaturation. For example, with 9.0 W ultrasonic power, the reduction in induction time was about 880 s (from 1270 s to 390 s, reduced by 69.29%) at the supersaturation ratio of 2.2, while at the supersaturation ratio of 3.0, the reduction was only about 41 s (from 201 s to 160 s, reduced by 20.40%). Therefore, the ultrasound could promote the nucleation significantly, particularly at lower supersaturation ratios. Similar results were also reported in other compound nucleation studies [41–43], and the results were shown in Table S5. As a result, the effect of ultrasound on the induction time is a universal phenomenon. In addition, there is a one-to-one correspondence between concentrations and supersaturation ratios, which is shown in Table S2. Thus, the variation of induction time with concentration follow the same rule with supersaturation ratios.

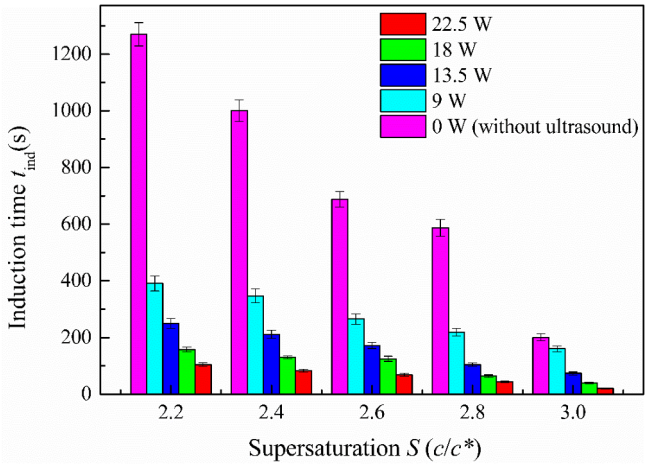


Fig. 1. The effect of continuous ultrasonic irradiation on the induction time of nucleation.

A series of pulsed ultrasonic irradiation was also investigated for the induction time measurement. The results attached in Supporting information (Fig. S1) illustrated an obvious nucleation enhancement, and the intensifying effect was strongly related to the duty cycle which would be recommended for the fine-tunning of nucleation kinetics. With constant power and supersaturation ratio, comparing Fig. 1 with Fig. S1, the continuous ultrasound was more powerful in promoting LGA nucleation than the pulsed ultrasound. Similarly, the variation of induction time with concentration follow the same trend with supersaturation ratios. The possible mechanism to explain the effect of ultrasound on induction time is generally attributed to the cavitation phenomena (being the formation, growth and collapse of cavitation bubbles) which is created by the pressure variation in the solutions [15]. The collapse of cavitation bubbles causes intense high pressure, as well as shockwaves, microjets and micro-turbulences in solution. The former causes local supersaturation and the latter increases the opportunity of collisions among solute molecules, which creates more clusters necessary for nucleation and thus accelerates the nucleation to obtain a shorter induction time [15,44,45]. With higher ultrasonic power, the cavitation activity is gradually enhanced, which accelerates the formation of local supersaturation, as well as the collisions among solute molecules for a quicker nucleation, resulting in a decrease of induction time. Similarly, in pulsed setting experiments, the longer ultrasonic working time per unit time could improve the cavitation activity per unit time, resulting in nucleation enhancement and induction time shortened. Thus, the ultrasound could accelerate the nucleation rate of crystallization system, especially for the system difficult to nucleate at lower supersaturation.

The MSZWs (ΔT_{max}) measured in the absence and presence of ultrasound were listed in Table 1. As shown in Table 1, the MSZWs were significantly reduced by the application of ultrasound (22.5 W), indicating that the supersaturated solution became more unstable under the ultrasound. As shown in Table S3, the ultrasound decreased the supersaturation ratios required for nucleation. The effect of ultrasound on MSZWs was more effective at lower cooling rates. For example, at 348.15 K, the MSZW was decreased by 55.88% (from 6.8 K to 3.0 K) at the cooling rate of 6 K/h, while at the cooling rate of 90 K/h the MSZW was only decreased by 30% (from 15.0 K to 10.5 K).

Similar mechanism with the effect of ultrasound on induction time, the collapse of cavitation bubbles generates very high local pressures, which creates local supersaturation being enough for nucleation, thus higher nucleation temperatures can be obtained, presenting narrower

Table 1
MSZWs of LGA in the absence and presence of ultrasound from 315.15 K to 348.15 K.

Solubility		ΔT_{max}/K (without ultrasound)				ΔT_{max}/K (22.5 W ultrasound)			
T_0/K	x_β	6 K/h	30 K/h	60 K/h	90 K/h	6 K/h	30 K/h	60 K/h	90 K/h
348.15	0.0055	6.8 ± 0.70	8.7 ± 0.62	12.4 ± 0.56	15.0 ± 0.62	3.0 ± 0.17	4.5 ± 0.40	6.6 ± 0.46	10.5 ± 0.44
344.15	0.0049	7.2 ± 0.53	9.3 ± 0.66	13.2 ± 0.66	16.0 ± 0.82	3.2 ± 0.20	5.0 ± 0.30	8.2 ± 0.44	13.5 ± 0.61
339.15	0.0043	7.8 ± 0.78	10.2 ± 0.60	14.2 ± 0.75	17.2 ± 0.75	3.6 ± 0.36	5.7 ± 0.26	10.5 ± 0.53	15.8 ± 0.60
334.15	0.0037	8.7 ± 0.44	11.5 ± 0.95	16.0 ± 0.78	20.5 ± 0.95	4.2 ± 0.35	7.8 ± 0.35	13.2 ± 0.30	18.9 ± 0.35
315.15	0.0018	10.2 ± 0.56	13.9 ± 0.96	20.3 ± 0.92	27.5 ± 0.66	5.4 ± 0.26	10.9 ± 0.36	16.7 ± 0.62	23.3 ± 0.46

MSZWs [15,45,46]. Jiang [26] also obtained the MSZWs of LGA during the cooling crystallization process (6 K/h cooling rate and 25 W ultrasonic power) in 500 mL working solution. Compared with the data obtained without ultrasound, the MSZW was reduced by an average of 41.01% in Jiang' study [26], which was a little lower than the value of 48.48% in present work. Thus, the difference in ultrasonic energy per unit working volume (0.05 W/mL in Jiang' study and 0.75 W/mL in present work) caused the different efficiency in nucleation.

3.2. Effects of ultrasound on nucleation parameters

To quantify the effects of ultrasound on crystal nucleation, the theoretical nucleation kinetics were calculated. According to the theory of regular solution, the relationship between c_0 and c_1 could be written as Eq. (1) [47]. The c_0 and c_1 represent the solute concentrations at saturation temperature T_0 and nucleation temperature T_1, respectively.

$$\ln\frac{c_0}{c_1} = \frac{\Delta H_s}{R_g T_1}\frac{\Delta T_{max}}{T_0} \tag{1}$$

ΔH_s is the change of dissolution enthalpy (kJ/mol) and R_g is the gas constant which equals 8.314 J/(mol·K). When the relative supersaturation $\sigma \ll 1$, $\ln S \approx \sigma$ ($\sigma = \Delta c/c_1 = (c_0 - c_1)/c_1$, $S = c_0/c_1$). The Eq. (2) can be expressed as:

$$\ln S = \frac{\Delta c}{c_1} = \frac{\Delta H_s}{R_g T_1}\frac{\Delta T_{max}}{T_0} \tag{2}$$

Sangwal [48] assumed that the nucleation rate J is related to the change of solution supersaturation $\Delta c/c_1$. Then the nucleation rate J ($m^{-3}\cdot s^{-1}$), can be characterized as follows

$$J = f\frac{\Delta c}{c_1 \Delta t} = f\frac{\Delta c}{c_1 \Delta T}\frac{\Delta T}{\Delta t} = f\frac{\Delta H_s}{R_g T_1}\frac{R}{T_0} \tag{3}$$

In this equation, the cooling rate R (K/h), can be written as $\Delta T/\Delta t$, and the proportionality constant f is concerned with aggregation and diffusion process in the solution, which is defined as the number of entities per unit volume [27,48]. Based on the classical theory of three-dimensional nucleation, the nucleation rate can be expressed as [49]

$$J = A\exp\left[-\frac{16\pi\gamma^3 V_s^2}{3k^3 T_1^3}\frac{1}{(\ln S)^2}\right] \tag{4}$$

According to Eq. (2), $1/(\ln S)^2$ can be expressed as:

$$(\ln S)^2 = \left(\frac{\Delta H_s}{R_g T_1}\frac{\Delta T_{max}}{T_0}\right)^2 \tag{5}$$

Combining Eq. (3) and Eq. (4) with Eq. (5),

$$\exp\left[-\frac{16\pi\gamma^3 V_s^2}{3k^3 T_1^3}\left(\frac{R_g T_1}{\Delta H_s}\right)^2\left(\frac{T_0}{\Delta T_{max}}\right)^2\right] = f\frac{\Delta H_s}{R_g T_1}\frac{R}{A T_0} \tag{6}$$

where the A is the pre-exponential factor ($m^{-3}\cdot s^{-1}$), related to the kinetics of formation of nuclei in the growth medium, and lies between 10^{15} and 10^{42}. Besides, V_s (m^3) is the molecule volume, γ (mJ/mol) represents the effective interfacial energy between liquid and solid, and k is Boltzmann constant which can be expressed as R_g/N_A (N_A is the Avogadro number). The Eq. (6) can be rearranged by taking logarithm on both sides and expressed as:

$$\left(\frac{T_0}{\Delta T_{max}}\right)^2 = F_1(X + \ln T_0 - \ln R) = F - F_1 \ln R \tag{7}$$

Among this equation, $F = F_1(X + \ln T_0)$

$$F_1 = \left[\frac{3k^3 T_1^3}{16\pi\gamma^3 V_s^2}\left(\frac{\Delta H_s}{R_g T_1}\right)^2\right] \tag{8}$$

$$X = \ln\left(\frac{A}{f}\frac{R_g T_1}{\Delta H_s}\right) \tag{9}$$

Eq. (7) reveals that there is a linear relationship between $(T_0/\Delta T_{max})^2$ and $\ln R$ at a given initial saturated concentration. According to Eq. (8), the interfacial energy γ can be determined by the slope of F_1.

Besides, the actual driving force for crystallization is the difference between the chemical potentials in the liquid phase (μ_l) and solid phase (μ_s), $\Delta\mu$, which can be calculated by Eq. (10):

$$\Delta\mu = \mu_l - \mu_s = kT\ln S = k\frac{\Delta H_s}{R_g}\frac{\Delta T_{max}}{T_0} \tag{10}$$

Based on the classical nucleation theory [40], critical nucleus size r_{crit} and critical Gibbs free energy ΔG_{crit} can be derived by combining the interfacial energy γ with Eq. (10).

$$r_{crit} = \frac{2\gamma V_s}{\Delta\mu} = \frac{2\gamma R_g V_s}{k\Delta H_s}\frac{T_0}{\Delta T_{max}} \tag{11}$$

$$\Delta G_{crit} = \frac{4\pi\gamma r_{crit}^2}{3} \tag{12}$$

According to the MSZW data in Table 1, linear relationships between $(T_0/\Delta T_{max})^2$ and $\ln R$ are described in Fig. 2 at different saturation temperatures (T_0) with and without ultrasound. This approach shows a good fit with the MSZW experimental data at five different temperatures, and the fitting analysis parameters were listed in Table S6.

In Fig. 2(b), with application of ultrasound, the maximum supercooling ΔT_{max} (MSZW) decreases, which increases the value of $(T_0/\Delta T_{max})^2$ compared with the case without ultrasound (Fig. 2(a)). The values of slope and intercept are both sensitive to T_0 and increase with increasing T_0, which are in agreement with other studies [27,50,51].

Values of the slope F_1, intercept F, as well as the ratio between F_1 and F with and without ultrasound, were obtained from Fig. 2 and listed in Table 2. The parameter F_1 depends on ΔH_s and γ, which is determined by the thermodynamics and solvation process. F depends on ΔH_s, γ, f and A, which is governed by the thermodynamics and kinetics process [48,51]. As shown in Table 2, the nucleation parameters F and F_1 significantly increase with the increase of saturation temperature T_0, due to the thermodynamic factors. In the case without ultrasound, F and F_1 respectively increase by 1.70 times (from 1497.841 to 4078.656) and 1.60 times (from 302.720 to 780.798), while in the case with ultrasound, F and F_1 respectively increase by 3.00 times (from 5366.454 to 21659.261) and 2.80 times (from 1214.559 to 4591.381). Thus, not only the values of F and F_1 with ultrasound are larger than the values

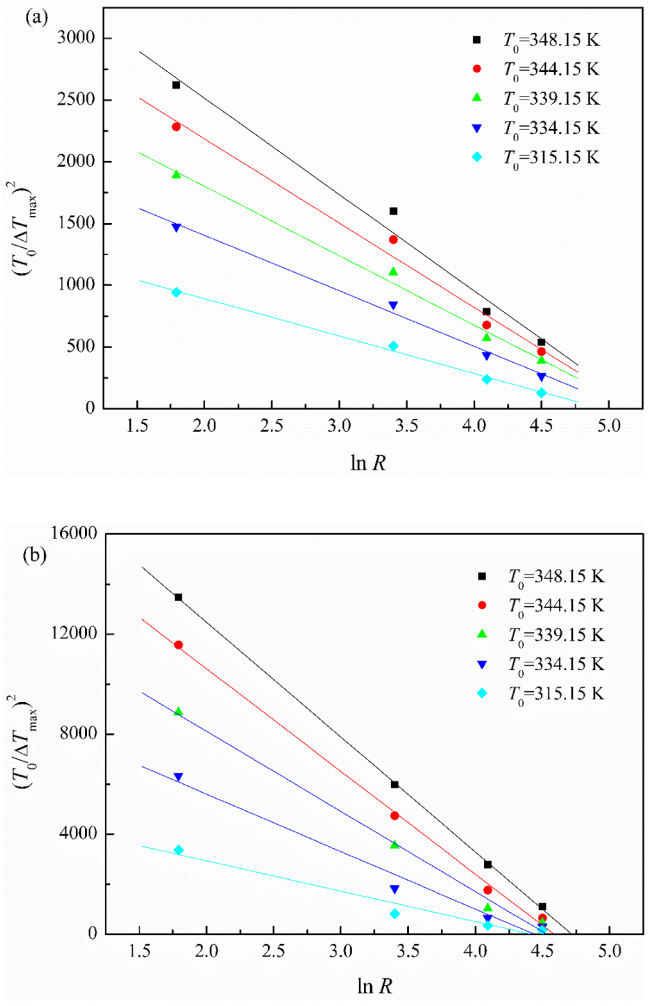


Fig. 2. The plot of $(\Delta T_0/\Delta T_{max})^2$ against ln$R$ for LGA: (a) without ultrasound; (b) 22.5 W ultrasound.

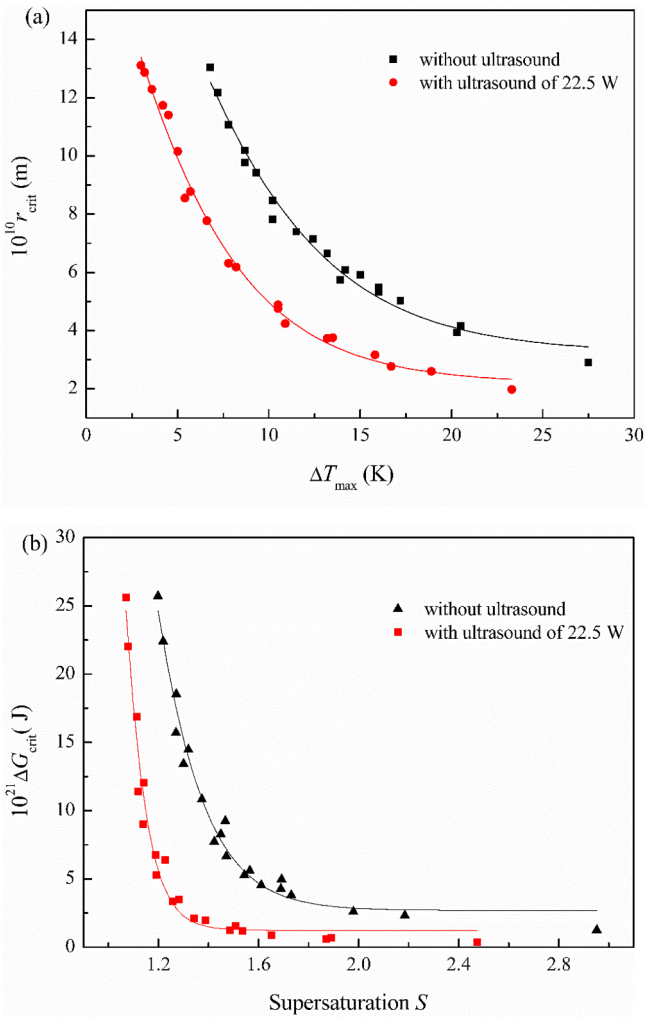


Fig. 3. (a) The plot of r_{crit} against ΔT_{max} with and without ultrasound in the solution; (b) The plot of ΔG_{crit} against supersaturation S with and without ultrasound in the solution. The solid lines represent the tendency of the data points.

without ultrasound, the multiples of the increases under ultrasound are larger. Except for enhancing the nucleation kinetics [26,27,41], the collapse of cavitation bubbles in the solutions also releases amounts of energy creating high local temperature [15,44] which may change local thermodynamics and increase the values of F and F_1. However, the effect of T_0 on F_1/F is limited, because F_1/F is a constant characteristic for a fixed compound representing for the growth rate of critical three-dimensional stable nuclei to detectable entities [48,51]. In addition, the value of F_1/F with ultrasound (0.22) is slightly larger than that without ultrasound (0.19), which indicates a larger growth rate of stable crystal nuclei is obtained in the ultrasound field. As a result, the ultrasound promotes the nucleation process.

Then the interfacial energy γ can be obtained by Eq. (8) and listed in Table S7, which have the same order of magnitude compared with other studies [13,41]. Compared to the values (from 3.18 mJ/m^2 to 4.23 mJ/m^2) without ultrasound, the values of γ (from 1.77 mJ/m^2 to 2.68 mJ/m^2) with ultrasound decrease by an average of 42.1%. The interfacial energy is a characterized parameter to describe the difficulty of nucleation spontaneously in solution, which is sensitive to the temperature and decreases with increase of saturation temperature [51,52]. In addition, the results also show a decline of γ in the presence of ultrasound, due to the increase of local temperature which is caused by the collapse of cavitation bubbles. Meanwhile, the low interfacial energy also reflects that the free energy difference between the crystal surface at the solution interface and the interior crystalline structure of the crystal is rather low [53]. Therefore, the solute could be easily crystallized from the solution because of easier nucleation. Finally,

Table 2
Nucleation parameters F, F_1 and F_1/F.

	Without Ultrasound				22.5 W Ultrasound			
T_0/K	F	F_1	F_1/F	R^2	F	F_1	F_1/F	R^2
348.15	4078.656	780.798	0.191	0.975	21659.261	4591.381	0.212	0.999
344.15	3553.511	683.068	0.192	0.980	18833.985	4106.787	0.218	0.996
339.15	2926.841	562.263	0.192	0.987	14531.516	3206.368	0.221	0.991
334.15	2303.540	449.177	0.195	0.989	10203.741	2299.003	0.225	0.962
315.15	1497.841	302.720	0.202	0.992	5366.454	1214.559	0.226	0.937

based on Eq. (11) and Eq. (12), the critical nucleus size r_{crit} and critical Gibbs free energy ΔG_{crit} are calculated and depicted in Fig. 3. Fig. 3(a) describes a plot of r_{crit} against maximum supercooling ΔT_{max} with and without ultrasound. The r_{crit} decreases exponentially with increasing ΔT_{max}, decreasing from 1.31 × 10^{-9} m to 1.98 × 10^{-10} m in sonicated solution and decreasing from 1.30 × 10^{-9} m to 2.9 × 10^{-10} m in unsonicated solution.

Fig. 3(b) describes a plot of ΔG_{crit} against supersaturation S with and without ultrasound. The ΔG_{crit} decreases exponentially with increasing S, decreasing from 2.56 × 10^{-20} J to 3.43 × 10^{-22} J in sonicated solution and decreasing from 2.57 × 10^{-20} J to 1.27 × 10^{-21} J in unsonicated solution. And the tendency lines of critical nucleus size and critical Gibbs free energy in the sonicated solution are both lower than that without ultrasound.

The results also point that the values of r_{crit} and ΔG_{crit} respectively decrease by an average of 4.5% and 29.2% in the crystallization process with the ultrasound implemented. The lower values of r_{crit} are directly related to the very low interfacial energy in the presence of ultrasound (no more than 2.7 mJ/m^2). Thus, the ultrasound decreases the critical size of stable nucleus facilitating the nucleation of solute. Usually, the ΔG_{crit} represents the total free energy change corresponding to the existence of the minimum-sized stable nucleus, above which the nucleus growth is thermodynamically favorable. In the current literatures about LGA crystallization in aqueous solution [26,39,54], Nývlt's approach [55] were applied to study the nucleation process. The nucleation parameters obtained by Nývlt's approach were the nucleation order (m) and nucleation rate constant (k_n), which were different from the nucleation parameters (γ, r_{crit} and ΔG_{crit}) in this study. To confirm the reliability of the results and discuss the results more adequately, the nucleation parameters were respectively calculated by Nývlt's approach and Sangwal's theory for comparison, which were shown in Table S8. The values of nucleation parameters were similar with these studies [26,39,54], and were in the same order of magnitude. In the presence of ultrasound, the variation tendencies of γ, r_{crit} and ΔG_{crit} in this study were also consistent with the results calculated from Jiang's study [26].

Therefore, the ultrasound applied to the solution reduces the minimum size for forming a stable nucleus, and further reduces the energy barrier needed for the continuous growth of the stable nucleus, which in turn explain the reason for the decrease of induction time and MSZWs in the presence of ultrasound.

3.3. Effect of ultrasound on polymorphic nucleation

The polymorphs of LGA could be identified by the difference of morphologies based on the microscope image [34], which was reconfirmed as shown in Fig. S2. Table 3 demonstrates that the pure β form crystals can be obtained in the stagnant condition despite the variations of other operating conditions such as initial concentrations and nucleation temperatures (T_1).

The absence of α form crystals may be caused by weak mass transfer in the solution without any agitation [37]. With 18.0 W ultrasound, the pure α form crystals can be produced in most cases, and a tendency line separating the metastable α form and stable β form is plotted in Table 3. Below the tendency line, the mixture of α form and the β form crystals is obtained, indicating that the β form prefers to nucleate at higher T_1 (≥308.15 K) under ultrasound. The nucleation rate of β form crystal becomes larger when the temperature is higher [37,26], which is also demonstrated in Fig. S3. The little difference in nucleation rate ($J_\beta \approx J_\alpha$) leads to the coexistence of both polymorphs.

Corresponding to the experimental conditions and results in Table 3, microscope images of LGA polymorphs distribution are shown in Fig. 4. Fig. 4(a) describes the morphology of β form LGA in the stagnant condition at the concentration of 45 mg/mL. With the increase of T_1 (corresponding to the decrease of S), the morphology of β form crystal tends to be plate-like shape without apparent aggregation. The similar phenomenon was reported by Roelands [38], in the reactive crystallization without any agitation, β form crystals were nucleated attributed to the occurrence of thermodynamically metastable droplets. And the size of the droplet decreased with decreasing supersaturation until the droplets could not be visible, leading to a difference in the morphology of β form crystals [38]. Fig. 4(b) describes the morphologies of LGA polymorph in sonicated condition at an initial concentration of 25 mg/mL. With an increase of the nucleation temperature from 273.15 K to 328.15 K, the morphology of LGA changes from prism shape (α form) to needle shape (β form), which is different from the stagnant condition. Besides, the polymorph distribution at experimental supersaturations followed the Oswald's rule of stages [21,56].

Table 4 describes the polymorphism distribution of LGA at the agitation rate of 200 rpm with different ultrasonic power during the process of quench cooling to 278.15 K. Similarly, a tendency line separating the metastable and stable form is plotted in Table 4. In the polymorphic distribution matrix, the pure α form crystals are crystallized at all the set of concentrations without ultrasound. While the nucleation of β form crystals prefer to occur at higher concentration (35 mg/mL and 45 mg/mL) and higher ultrasonic power (> 9.0 W). Thus, except for the temperature, the solution concentration also affects the LGA polymorph nucleation.

During the cooling process, the ultrasound increases the nucleation temperature and causes an increase in J_β. When the ultrasonic power attains a certain value, the J_β may be a little higher than the J_α. Thus, the pure β form crystals could be easily crystallized with higher ultrasonic power, *e.g.*, at the concentration of 45 mg/mL with 27.0 W ultrasound. The similar polymorphic control was presented in the crystallization of paracetamol, and the metastable form II form was produced with application of ultrasound, increasing the local supersaturation for the form II nucleation and enhancing the nucleation rates of form II [21]. Except for the effect of nucleation kinetics (affected by ultrasound) on the polymorph crystallization [21,22,30], there is another way to explain the preferential crystallization of one polymorph. For example, in the crystallization process of p-aminobenzoic acid, the

Table 3
Polymorphism distribution of LGA crystals at various concentrations without any magnetic agitation and with 18.0 W ultrasound in the solution.

T_1/K	Stagnant condition				18.0 W ultrasound			
	45 mg/mL	35 mg/mL	25 mg/mL	15 mg/mL	45 mg/mL	35 mg/mL	25 mg/mL	15 mg/mL
273.15 K	β	β	β	β	α	α	α	α
298.15 K	β	β	β	--	α	α	α	--
308.15 K	β	β	β	--	α	α	α+β	--
318.15 K	β	β	β	--	α	α+β	β	--
328.15 K	β	β	--	--	α+β	α+β	--	--

"–" represents none: crystal nucleation did not occur after 3 h.

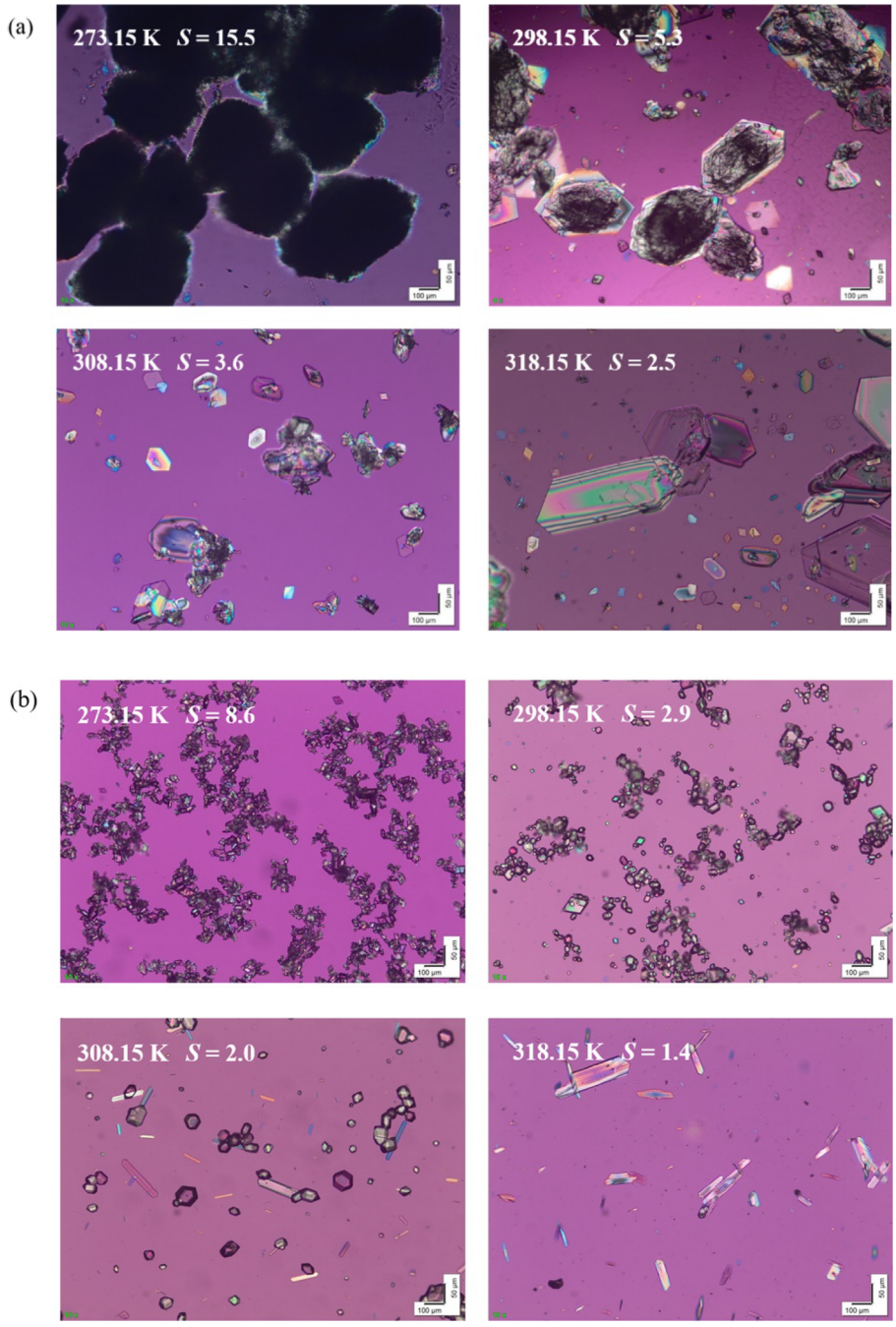


Fig. 4. Microscope images of (a) β form crystals in stagnant condition at initial concentration of 45 mg/mL; (b) LGA polymorphs under 18.0 W ultrasound at initial concentration of 25 mg/mL.

Table 4
Polymorphism distribution of LGA with various concentrations and ultrasonic power during the process of quench cooling to 278.15 K.

	200 rpm with ultrasonic irradiation			
Power	45 mg/mL	35 mg/mL	25 mg/mL	15mg/mL
0 W	α	α	α	α
7.2 W	α	α	α	α
9.0 W	α+β	α	α	α
13.5 W	α+β	α+β	α	α
27.0 W	β	α+β	α	α

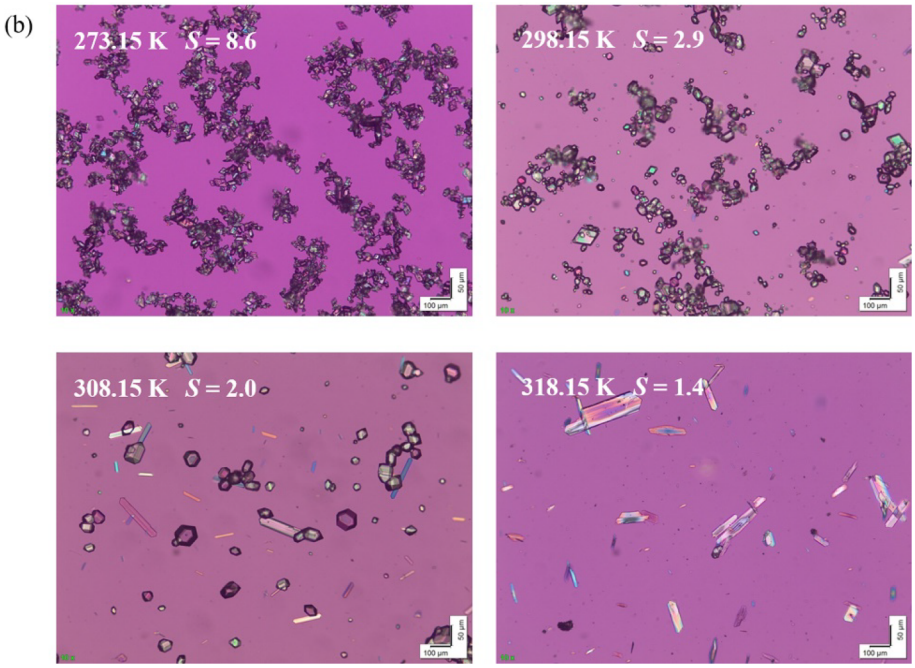


Fig. 5. Microscope images of LGA polymorphism at a concentration of 45 mg/mL corresponding to the conditions in Table 4.

centro symmetric dimer precursors (α form) were decreased by ultrasonic energy, which increased the opportunity of the other precursors (β form) occurrence in solution [24]. However, in the study of glycine crystallization [13], the nucleation of α form crystals (with dimers as the basic building units) were promoted by the ultrasound, which was opposite with the results obtained by studying p-aminobenzoic acid [24]. Therefore, in the ultrasound assisted nucleation process, the mechanisms for polymorph control of different compounds are not unified. The microscope images in Fig. 5 show the distributed polymorphism corresponding to the experimental conditions in Table 4. With an increase of the ultrasonic power (0–27.0 W), the morphologies of LGA change from prism shape (α form) to needle shape (β form), which indicates an effective manipulation of polymorphism by ultrasound.

The effect of ultrasound on LGA polymorphic control can be summarized as follows: (1) The ultrasound irradiation could act as an agitation which enhances the mass transfer in the solution to produce α form crystals, comparing with the products (pure β form crystals) in the stagnant solution. (2) The β form crystals could nucleate with certain ultrasonic power at the concentrations where α form crystals prefer to occur without the ultrasound. Under some conditions, the stable β form crystals could be produced just by nucleation, excluding the influence of solvent-mediated polymorphic transformation (from the metastable α form to the stable β form). Due to the quench cooling process, the transformation time is eliminated, and the product polymorphism reflects the polymorphic situation of LGA in the nucleation stage.

3.4. Effect of ultrasound on the polymorphic transformation

In this section, the LGA polymorphic transformation process (from α to β form) was tracked by *in-situ* Raman spectroscopy and PXRD during the polymorphic transformation process with and without ultrasound.

The α and β form crystals were characterized by Raman spectroscopy both in solid-state and aqueous suspension. The Raman spectra in solid-state and aqueous suspension were depicted in Fig. S4, which indicated the apparent difference in the characteristic peaks between α (871.1 cm^{-1}) and β (417.3 cm^{-1}) form crystals. With 27.0 W ultrasound, *in-situ* Raman spectra of α and β form crystals were extracted by deducting the solvent spectrum background, as shown in Fig. 6. The intensity of α form characteristic peak located at 871.1 cm^{-1} decreased (Fig. 6a) and the intensity of β form characteristic peak located at 417.3 cm^{-1} increased (Fig. 6b) along with the proceeding of the process, which illustrated the transformation from α to β form. After two hours, the characteristic peak intensity of α and β form crystals reached a plateau, which indicated the completion of the polymorphic transformation process with 27.0 W ultrasound.

Through a series of experiments by varying the ultrasonic power (0–27.0 W), it is found that the polymorphic transformation process can be accelerated by ultrasound, and the increase of ultrasonic power can further intensify the transformation process. As indicated in Fig. 7(a), the process without ultrasound requires 600 min to complete the polymorphic transformation, while in Fig. 7(b), it only requires 210 min to complete the transformation process with 7.2 W ultrasound. The intensification of polymorphic transformation by ultrasonic irradiation could bring significant benefits for polymorphic control and improving process efficiency in practical manufacturing. With the continuous increase of ultrasonic power, as shown in Fig. 7(c) and (d), the transformation time was further reduced to 150 min and 120 min under 13.5 W and 27.0 W ultrasound, respectively. While the further increase of ultrasonic power should be careful as the transformation would not be intensified infinitely, and the temperature would be hard to control during the experiment. Thus, the quantitative analysis is required to understand the polymorphic transformation kinetics with and without ultrasound and optimize the effective ultrasonic power to intensify the transformation process.

PXRD was used to characterize the composition of the crystal polymorph during the polymorphic transformation process with and without ultrasonic irradiation. Ten samples were collected to determine the polymorph composition in every experiment. A representative result of ultrasound-assisted polymorphic transformation at 27.0 W is shown in Fig. 8. The peaks of 18.0° and 26.6° are tracked as the characteristic peaks of α form, and the peak located at 10.0° is tracked for β form. At the time of 0 min, only the characteristic peak of α form appeared in the PXRD pattern, indicating that only the pure α form was present in solution at the beginning of the transformation process. As time went on, the intensity of α form characteristic peak decreased, and the intensity of β form characteristic peak increased gradually. About two hours later, the characteristic peaks of α form disappeared, and the peaks of β form reached the constant value to complete the

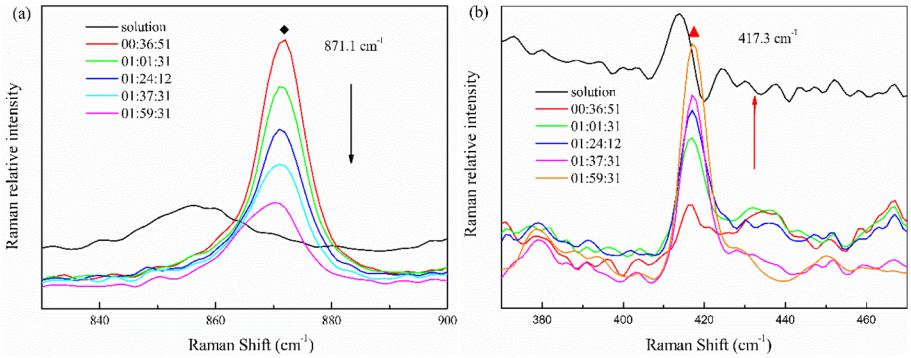


Fig. 6. The changes of *in-situ* Raman characteristic peaks intensity in the process of solvent-mediated phase transformation with 27.0 W ultrasound at 318.15 K: (a) Raman relative intensities of α form; (b) Raman relative intensities of β form.

polymorphic transformation process, which is consistent with the *in-situ* Raman tracking in Fig. 7(d). In further, comprehensive studies were conducted to investigate the effect of different ultrasonic power (0 W, 7.2 W and 13.5 W) on polymorphic transformation, and results are indicated in Fig. S5, which are consistent with the results in Fig. 7.

Based on the PXRD data, quantitative analyses of polymorphic transformation can be developed by the mass fractions of α and β form crystals. The mass fractions of two crystal forms were calculated by the change of the characteristic peak intensity using Eq. (13) and Eq. (14) [57]. Among these equations, X_A and X_B represent the mass fraction of α form and β form, respectively. I_{iA} and I_{jB} stand for the characteristic peak intensity of α form and β form, and I_A° and I_B° stand for the characteristic peak intensity of the pure α form and β form, respectively. According to the Avrami-Erofeev model in Eq. (15), which is widely used in the quantification of phase transformation, the polymorphic transformation kinetics in the transformation process can be obtained [58]. X and t respectively represent the mass fraction of LGA and transformation time. The k and n stand for the rate constant and Avrami exponent, respectively.

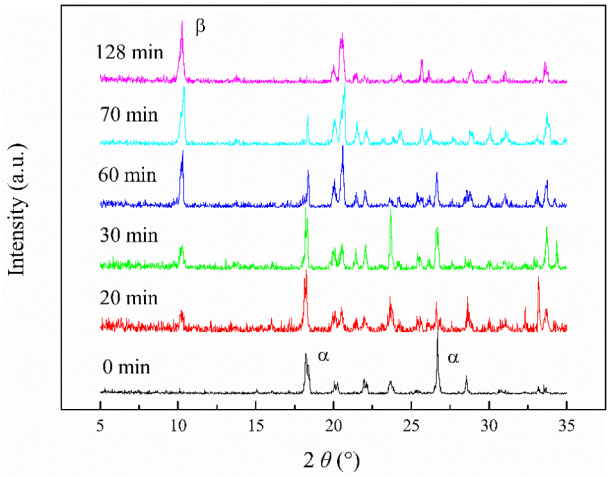


Fig. 8. PXRD patterns during the transformation process with 27.0 W ultrasound.

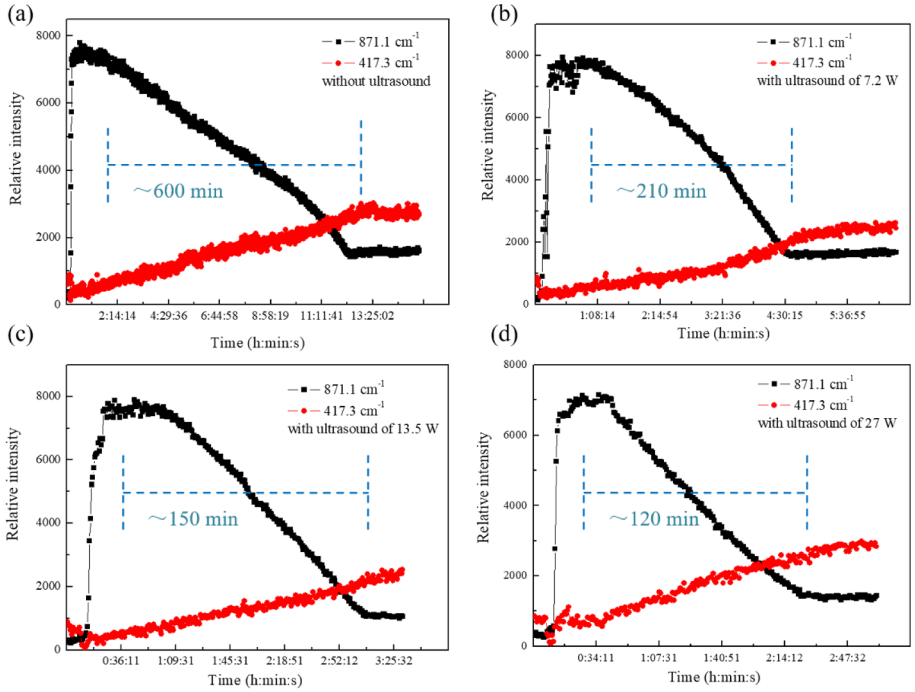


Fig. 7. *In-situ* Raman spectra of solvent-mediated phase transformation from α form to β form at 318.15 K: (a) without ultrasound; (b) 7.2 W ultrasonic power; (c) 13.5 W ultrasonic power; (d) 27.0 W ultrasonic power.

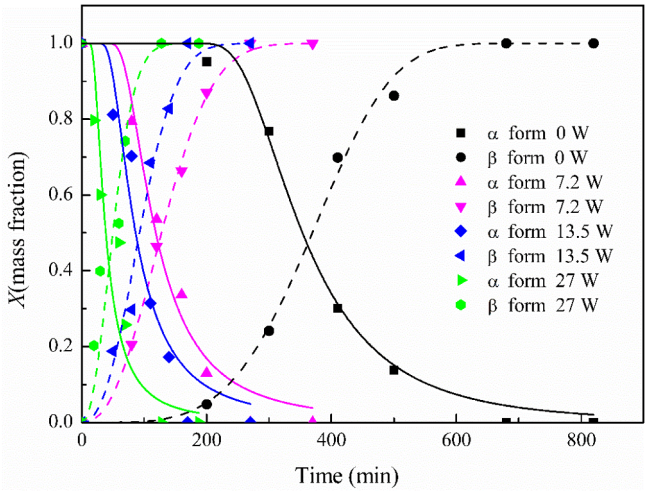


Fig. 9. Plots of transformation kinetics analysis at different ultrasonic power: 0 W, 7.2 W, 13.5 W and 27.0 W.

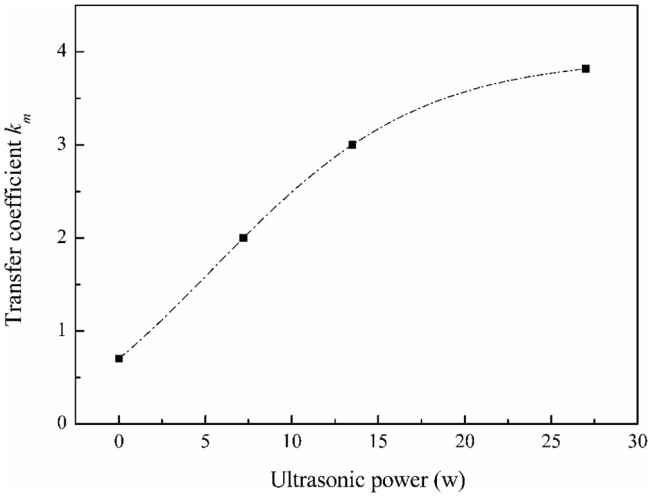


Fig. 11. Mass transfer coefficient k_m changes with ultrasonic power. The dashed line represents the tendency of the data points.

$$X_A = \frac{I_{iA}}{(I_{iA} + /_{jB}(I_A^{\circ}/I_B^{\circ}))} \tag{13}$$

$$X_B = \frac{I_{jB}}{(I_{jB} + I_{iA}(I_B^{\circ}/I_A^{\circ}))} \tag{14}$$

$$X = 1 - \exp[-(k\times t)^n] \tag{15}$$

Fig. 9 illustrates the changing of transformation kinetics along with the varying of ultrasonic power and fitting analysis parameters were listed in Table S9. The transformation time has a significant decline when ultrasound is applied (600–120 min). Before a sharp decrease of the curve, there is a plateau time which is the induction time of β form. And it indicates that the induction time was also significantly shortened with application of ultrasound, *e.g.*, from 220 min with 0 W ultrasound to 5 min with 27.0 W ultrasound.

By correlating the Avrami-Erofeev model (Eq. (15)) with experimental data, model parameters k and n are obtained and described in Fig. 10. The k represents the transformation rate, and n reflects the crystallization mechanism in the transformation process, which usually decreases with the increase of nucleation rate [59]. The Avrami exponent n stands for the number of growth dimensions. For instance, $n = 2$ and $n = 3$ correspond to two-dimensional and three-dimensional growth of nuclei, and $n = 4$ represents three-dimensional growth with a constant nucleation rate which can be regarded as a growth dimension [57,60]. In Fig. 10, the Avrami exponent n changes from 4 to 2 with application of ultrasound from 0 W to 27.0 W, which indicates the nucleation of stable form is no longer an element in the rate-limiting step, and the growth mechanism changed from three- to two-dimension. The theoretical results well explained the experimental results that both the induction time of β form crystal and the transformation time were shortened, as shown in Fig. 9. And it is also consistent with the conclusion that the nucleation and growth of the β form are the rate-limiting steps in the polymorph transformation of LGA [61].

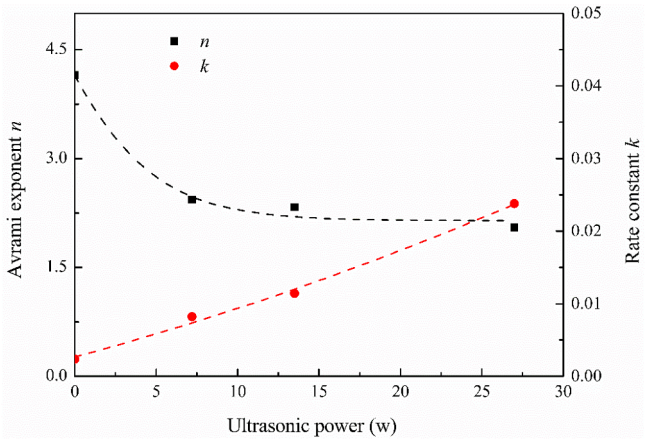


Fig. 10. Avrami-Erofeev model parameters k and n change with ultrasonic power. The dashed lines represent the tendency of the data points.

There is an obvious increase of the transformation rate constant k, and the reasons for the increase can be summarized as follows: (1) According to the nucleation parameters calculated by MSZWs data, the solid–liquid surface energy decreases with the application of ultrasonic irradiation, thus the nucleation of β form could be enhanced; (2) As the β form prefers to nucleate on the surface of α form in aqueous solution [62,63], the application of ultrasound in the suspension liquid increases attrition of α form crystals and creates more surface area as the nucleation sites to facilitate the nucleation of β form crystals; (3) Meanwhile, the mass transfer in solution which is important in the transformation process has also been intensified with the application of ultrasonic irradiation. The total amount of β form crystals (m) during the transformation process has a relationship with mass transfer rate (r) and transformation time t_T, which could be shown as $m \sim r \cdot t_T$ [64]. The mass transfer rate (r) is concerned with the mass transfer coefficient (k_m) and concentration difference (ΔC), which could be presented as $r \sim k_m \cdot \Delta C$ [64]. Hence, the changing of k_m with different ultrasonic power is shown in Fig. 11. As indicated in the result, the calculated mass transfer coefficient (3.8) with the 27.0 W ultrasonic power is 5 times as large as the coefficient (0.7) without ultrasound. The higher ultrasonic power would induce a larger k_m and promote the nucleation and growth of β form crystals, thereby accelerating the polymorphic transformation process.

To analyze the reasonability of the above results, the comparison with other studies [65–67] is conducted, which is shown in Table S10. In 2004, Ono et al. [65] ignored the primary nucleation of β form crystals in the LGA transformation process ($S \leq 2.4$). Due to that the purity of α form crystals applied in the experiments was about 80%-100%, the β form crystals may exist at the beginning of the transformation process. Thus, the study provided that the growth of the β form crystals was the rate-limiting step in the transformation process [65]. In 2006, Schöll et al. [66] concluded that the nucleation and growth the β form were the rate-limiting steps in the LGA transformation process ($S \geq 2.5$). In 2008, Dharmayat et al. [67] discussed the LGA transformation kinetics with online powder X-ray diffraction. The author did not consider the primary nucleation of the β form crystal in the kinetic

model, and concluded that the growth of the β form crystal was the rate-limiting step in the transformation process [67]. In the present study (S = 2.6), based on the Avrami-Erofeev model, the rate-limiting step of LGA transformation process without ultrasound was determined to be the nucleation and growth of the β form crystals, which was consistent with above studies [65–67].

In the presence of ultrasound, the rate-limiting step was changed from the nucleation and growth of β form crystals to the growth of β form crystals. The effect of β crystal nucleation on the transformation process was weakened by the ultrasound, which was significantly reflected by the shortened induction time of β form crystals. As a result, the transformation mechanism affected by ultrasound could provide references and guidance for other similar studies.

4. Conclusion

This work investigated the effects of ultrasound on crystal nucleation, polymorphic control and polymorphic transformation of LGA in detail. The results indicated the induction time and MSZWs were shortened with application of ultrasound, and the induction time was further shortened with higher ultrasonic power. The nucleation parameters calculated by MSZWs data, such as the interfacial energy, critical nucleus size, and critical Gibbs free energy, were decreased significantly in the presence of ultrasound. The promotion of ultrasound-assisted nucleation can be attributed to decreasing the smallest size of the crystal nucleus capable of continued growth and reducing the energy barrier for nucleation. Without magnetic agitation, the pure α form crystal could be produced with 18.0 W ultrasonic power due to the enhancement of the mass transfer in solution. In addition, the combination of ultrasonic power and solution concentration affected the nucleation of β form crystals. The products could reflect the actual polymorph distribution in the nucleation stage.

Furthermore, the mechanism of solvent-mediated polymorphic transformation kinetics with ultrasound was discussed using Avrami-Erofeev model for the first time. Due to the change of crystallization mechanism (nucleation and growth of β form crystals) in the transformation process, the transformation rate was highly improved to 2.8–5 times compared with the results without ultrasound. The study presented in-depth understanding of the mechanism of ultrasound-assisted LGA crystallization, and the quantitative analysis would provide a better control for the ultrasound-assisted crystallization intensification.

CRediT authorship contribution statement

Chen Fang: Investigation, Writing - original draft, Data curation, Formal analysis. **Weiwei Tang:** Conceptualization, Validation. **Songgu Wu:** Resources. **Jingkang Wang:** Funding acquisition, Project administration. **Zhenguo Gao:** Writing - review & editing, Supervision. **Junbo Gong:** . **:** Funding acquisition, Project administration.

Declaration of Competing Interest

The authors declare that they have no known competing financial interests or personal relationships that could have appeared to influence the work reported in this paper.

Acknowledgments

The authors are grateful to the financial support of the National Natural Science Foundation of China (NOs. NNSFC 21808159 and 21676179), the National Key Research and Development Program of China (No. 2020BZ-0005), the open foundation of the State Key Laboratory of Chemical Engineering (NO. SKL-ChE-18B04), and Major National Science and Technology Projects 2017ZX09101001.

Appendix A. Supplementary data

Supplementary data to this article can be found online at https://doi.org/10.1016/j.ultsonch.2020.105227.

References

[1] M. Maghsoodi, Role of solvents in improvement of dissolution rate of drugs: crystal habit and crystal agglomeration, Adv. Pharm. Bull. 5 (2015) 13–18.
[2] E.S. Ferrari, R.J. Davey, W.I. Cross, A.L. Gillon, C.S. Towler, Crystallization in polymorphic systems: the solution-mediated transformation of β to α glycine, Cryst. Growth Des. 3 (2003) 53–60.
[3] M. Maghsoodi, How spherical crystallization improves direct tableting properties: a review, Adv. Pharm. Bull. 2 (2012) 253–257.
[4] T. Beyer, G.M. Day, S.L. Price, The prediction, morphology, and mechanical properties of the polymorphs of paracetamol, J. Am. Chem. Soc. 123 (2001) 5086–5094.
[5] M. Kitamura, Strategy for control of crystallization of polymorphs, CrystEngComm. 11 (2009) 949–964.
[6] G. Madras, B.J. McCoy, Growth and ripening kinetics of crystalline polymorphs, Cryst. Growth Des. 3 (2003) 981–990.
[7] A.W. Xu, W.F. Dong, M. Antonietti, H. Cölfen, Polymorph switching of calcium carbonate crystals by polymer-controlled crystallization, Adv. Funct. Mater. 18 (2008) 1307–1313.
[8] R.K. Garg, D. Sarkar, Polymorphism control of p-aminobenzoic acid by isothermal anti-solvent crystallization, J. Cryst. Growth 454 (2016) 180–185.
[9] J.V. Parambil, S.K. Poornachary, R.B.H. Tan, J.Y.Y. Heng, Template-induced polymorphic selectivity: the effects of surface chemistry and solute concentration on carbamazepine crystallization, CrystEngComm. 16 (2014) 4927–4930.
[10] J. Zaccaro, J. Matic, A.S. Myerson, B.A. Garetz, Nonphotochemical, laser-induced nucleation of supersaturated aqueous glycine produces unexpected γ-polymorph, Cryst. Growth Des. 1 (2001) 5–8.
[11] F. Li, R. Lakerveld, Electric-field-assisted protein crystallization in continuous flow, Cryst. Growth Des. 18 (2018) 2964–2971.
[12] N. Amara, B. Ratsimba, A.M. Wilhlm, H. Delmas, Crystallization of potash alum: effect of power ultrasound, Ultrason. Sonochem. 8 (2001) 265–270.
[13] K.R. Devi, A. Raja, K. Srinivasan, Ultrasound assisted nucleation and growth characteristics of glycine polymorphs-a combined experimental and analytical approach, Ultrason. Sonochem. 24 (2015) 107–113.
[14] A.A. Thorat, S.V. Dalvi, Ultrasound-assisted modulation of concomitant polymorphism of curcumin during liquid antisolvent precipitation, Ultrason. Sonochem. 30 (2016) 35–43.
[15] S. Nalesso, M.J. Bussemaker, R.P. Sear, M. Hodnett, J. Lee, A review on possible mechanisms of sonocrystallisation in solution, Ultrason. Sonochem. 57 (2019) 125–138.
[16] J. Lee, K. Yasui, M. Ashokkumar, S.E. Kentish, Quantification of cavitation activity by sonoluminescence to study the sonocrystallization process under different ultrasound parameters, Cryst. Growth Des. 18 (2018) 5108–5115.
[17] J.F. Jia, W.C. Wang, Y. Gao, Y.P. Zhao, Controlled morphology and size of curcumin using ultrasound in supercritical CO_2 antisolvent, Ultrason. Sonochem. 27 (2015) 389–394.
[18] S.R. Iyer, P.R. Gogate, Ultrasound assisted crystallization of mefenamic acid: effect of operating parameters and comparison with conventional approach, Ultrason. Sonochem. 34 (2017) 896–903.
[19] S. Nii, S. Takayanagi, Growth and size control in anti-solvent crystallization of glycine with high frequency ultrasound, Ultrason. Sonochem. 21 (2014) 1182–1186.
[20] R.S. Vishwakarma, P.R. Gogate, Intensified oxalic acid crystallization using ultrasonic reactors: understanding effect of operating parameters and type of ultrasonic reactor, Ultrason. Sonochem. 39 (2017) 111–119.
[21] S.K. Bhangu, M. Ashokkumar, J. Lee, Ultrasound assisted crystallization of paracetamol: crystal size distribution and polymorph control, Cryst. Growth Des. 16 (2016) 1934–1941.
[22] Y. Ike, I. Hirasawa, Polymorph control of L-phenylalanine in cooling crystallization by ultrasonication, Chem. Eng. Technol. 41 (2018) 1093–1097.
[23] B.W. Zeiger, K.S. Suslick, Sonofragmentation of molecular crystals, J. Am. Chem. Soc. 133 (2011) 14530–14533.
[24] S. Gracin, M.U. Penttilä, Å.C. Rasmuson, Influence of ultrasound on the nucleation of polymorphs of p-aminobenzoic acid, Cryst. Growth Des. 5 (2005) 1787–1794.
[25] G.S. Zeng, H. Li, S.L. Luo, X.Y. Wang, J.H. Chen, Effects of ultrasonic radiation on induction period and nucleation kinetics of sodium sulfate, Korean J. Chem. Eng. 31 (2014) 807–811.
[26] S.Y. Jiang, An Examination of Sonocrystallization Kinetics of L-glutamic Acid, University of Leeds, 2012.
[27] T.H. Mastan, M. Lenka, D. Sarkar, Nucleation kinetics from metastable zone widths for sonocrystallization of L-phenylalanine, Ultrason. Sonochem. 36 (2017) 497–506.
[28] Y. Mori, M. Maruyama, Y. Takahashi, K. Ikeda, S. Fukukita, H.Y. Yoshikawa, S. Okada, H. Adachi, S. Sugiyama, K. Takano, S. Murakami, H. Matsumura, T. Inoue, M. Yoshimura, Y. Mori, Selective crystallization of metastable phase of acetaminophen by ultrasonic irradiation, Appl. Phys. Express. 8 (2015) 065501.
[29] S. Polat, P. Sayan, Effect of ultrasonic irradiation on morphology and polymorphic transformation of glycine, Ultrason. Sonochem. 47 (2018) 17–28.
[30] M. Kurotani, I. Hirasawa, Polymorph control of sulfamerazine by ultrasonic irradiation, J. Cryst. Growth 310 (2008) 4576–4580.

[31] H. Wu, N.R. McLaren, S. Jones, R.I. Ristic, J.P.A. Fairclough, A.R. West, Phase transformations of glutamic acid and its decomposition products, Cryst. Growth Des. 10 (2009) 988–994.
[32] Y.X. Mo, L.P. Dang, H.Y. Wei, L-glutamic acid polymorph control using amino acid additives, Ind. Eng. Chem. Res. 50 (2011) 10385–10392.
[33] E.S. Ferrari, R.J. Davey, Solution-mediated transformation of α to β L-glutamic acid: rate enhancement due to secondary nucleation, Cryst. Growth Des. 4 (2004) 1061–1068.
[34] Z.G. Gao, D. Zhu, Y.Y. Wu, S. Rohani, J.B. Gong, J.K. Wang, Motion-based multiple object tracking of ultrasonic-induced nucleation: a case study of L–glutamic acid, Cryst. Growth Des. 17 (2017) 5007–5011.
[35] N.C.S. Kee, R.B.H. Tan, R.D. Braatz, Selective crystallization of the metastable α-form of L-glutamic acid using concentration feedback control, Cryst. Growth Des. 9 (2009) 3044–3051.
[36] H. Hatakka, H. Alatalo, M. Louhi-Kultanen, I. Lassila, E. Haeggstrom, Closed-loop control of reactive crystallization part II: polymorphism control of L-glutamic acid by sonocrystallization and seeding, Chem. Eng. Technol. 33 (2010) 751–756.
[37] Y. Tahri, E. Gagnière, E. Chabanon, T. Bounahmidi, D. Mangin, Investigation of the L-glutamic acid polymorphism: comparison between stirred and stagnant conditions, J. Cryst. Growth 435 (2016) 98–104.
[38] C.P.M. Roelands, J.H. ter Horst, H.J.M. Kramer, P.J. Jansens, Precipitation mechanism of stable and metastable polymorphs of L-glutamic acid, AIChE J. 53 (2007) 354–362.
[39] X.W. Ni, A. Liao, Effects of cooling rate and solution concentration on solution crystallization of L-glutamic acid in an oscillatory baffled crystallizer, Cryst. Growth Des. 8 (2008) 2875–2881.
[40] J.W. Mullin, 5-Nucleation, in: J.W. Mullin (Ed.), Crystallization, fourth ed., Butterworth-Heinemann, Oxford, 2001, pp. 181–215.
[41] S.V. Dalvi, M.D. Yadav, Effect of ultrasound and stabilizers on nucleation kinetics of curcumin during liquid antisolvent precipitation, Ultrason. Sonochem. 24 (2015) 114–122.
[42] Z. Guo, M. Zhang, H. Li, J. Wang, E. Kougoulos, Effect of ultrasound on antisolvent crystallization process, J. Cryst. Growth 273 (2005) 555–563.
[43] N. Lyczko, F. Espitalier, O. Louisnard, J. Schwartzentruber, Effect of ultrasound on the induction time and the metastable zone widths of potassium sulphate, Chem. Eng. J. 86 (2002) 233–241.
[44] J.R.G. Sander, B.W. Zeiger, K.S. Suslick, Sonocrystallization and sonofragmentation, Ultrason. Sonochem. 21 (2014) 1908–1915.
[45] J. Jordens, B. Gielen, C. Xiouras, M.N. Hussain, G.D. Stefanidis, L.C.J. Thomassen, L. Braeken, T.V. Gerven, Sonocrystallisation: observations, theories and guidelines, Chem. Eng. Process.: Process Intesif. 139 (2019) 130–154.
[46] Z. Zhang, D.W. Sun, Z.W. Zhu, L. Cheng, Enhancement of crystallization processes by power ultrasound: current state-of-the-art and research advances, Comp. Rev. Food Sci. Food Safety 14 (2015) 303–316.
[47] S.J. Xu, J.K. Wang, K.K. Zhang, S.G. Wu, S.Y. Liu, K.L. Li, B. Yu, J.B. Gong, Nucleation behavior of eszopiclone-butyl acetate solutions from metastable zone widths, Chem. Eng. Sci. 155 (2016) 248–257.
[48] K. Sangwal, Novel approach to analyze metastable zone width determined by the polythermal method: physical interpretation of various parameters, Cryst. Growth Des. 9 (2009) 942–950.
[49] H.Y. Yang, A.J. Florence, Relation between metastable zone width and induction time of butyl paraben in ethanol, CrystEngComm. 17 (2015) 577–586.
[50] M. Luo, C.L. Liu, J. Xue, P. Li, J.G. Yu, Determination of metastable zone width of potassium sulfate in aqueous solution by ultrasonic sensor and FBRM, J. Cryst. Growth 469 (2017) 144–153.
[51] S.W. You, Y.F. Zhang, Y. Zhang, Nucleation of ammonium aluminum sulfate dodecahydrate from unseeded aqueous solution, J. Cryst. Growth 411 (2015) 24–29.
[52] Y. Zhao, G.Y. Hou, V.K. Kamaraju, Y.L. He, G. Power, B. Glennon, Primary nucleation of benzoic acid in aqueous ethanol solution, Ind. Eng. Chem. Res. 59 (2020) 484–490.
[53] R.A. Granberg, C. Ducreux, S. Gracin, Å.C. Rasmuson, Primary nucleation of paracetamol in acetone water mixtures, Chem. Eng. Sci. 56 (2001) 2305–2313.
[54] K.P. Liang, G. White, Derek Wilkinson, Examination of the process scale dependence of L-glutamic acid batch crystallized from supersaturated aqueous solutions in relation to reactor hydrodynamics, Ind. Eng. Chem. Res. 43 (2004) 1227–1234.
[55] J. Nývlt, Kinetics of nucleation in solutions, J. Cryst. Growth 4 (1968) 377–383.
[56] M. Ghosh, V. Venkatesan, S. Mandave, S. Banerjee, N. Sikder, A.K. Sikder, B. Bhattacharya, Probing crystal growth of ε- and α–CL-20 polymorphs via metastable phase transition using microscopy and vibrational spectroscopy, Cryst. Growth Des. 14 (2014) 5053–5063.
[57] Y.P. Wang, P.P. Sun, S.J. Xu, S.C. Du, T. Zhang, B. Yu, S.X. Zhang, Y. Wang, Y.W. Wang, J.B. Gong, Solution-mediated phase transformation of argatroban: ternary phase diagram, rate-determining step, and transformation kinetics, Ind. Eng. Chem. Res. 56 (2017) 4539–4548.
[58] D.L.T. Nguyen, K.J. Kim, Solvent-mediated polymorphic transformation of α-taltirelin by seeded crystallization, Chem. Eng. Technol. 39 (2016) 1281–1288.
[59] Y. Nishida, F. Aiga, S. Itoh, Microstructual path analysis of polycrystalline solidification by using multi-phase-field method incorporating a nucleation model, J. Cryst. Growth 405 (2014) 110–121.
[60] E.L. Pang, N.Q. Vo, T. Philippe, P.W. Voorhees, Modeling interface-controlled phase transformation kinetics in thin films, J. Appl. Phys. 117 (2015) 175304.
[61] J. Cornel, C. Lindenberg, M. Mazzotti, Experimental characterization and population balance modeling of the polymorph transformation of L-glutamic acid, Cryst. Growth Des. 9 (2009) 243–252.
[62] C. Cashell, D. Corcoran, B.K. Hodnett, Secondary nucleation of the β-polymorph of L-glutamic acid on the surface of α-form crystals, Chem. Commun. 3 (2003) 374–375.
[63] S.S. Liang, X.Z. Duan, X.Y. Zhang, G. Qian, X.G. Zhou, Supersaturation-dependent polymorphic outcome and transformation rate of L-glutamic acid, RSC Adv. 6 (2016) 74700–74703.
[64] J.H. An, G.J. Choi, W.S. Kim, Polymorphic and kinetic investigation of adefovir dipivoxil during phase transformation, Int. J. Pharm. 422 (2012) 185–193.
[65] T. Ono, H.J.M. Kramer, J.H. ter Horst, P.J. Jansens, Process modeling of the polymorphic transformation of L-glutamic acid, Cryst. Growth Des. 4 (2004) 1161–1167.
[66] J. Schöll, D. Bonalumi, L. Vicum, M. Mazzotti, In situ monitoring and modeling of the solvent-mediated polymorphic transformation of L-glutamic acid, Cryst. Growth Des. 6 (2006) 881–891.
[67] S. Dharmayat, R.B. Hammond, X.J. Lai, C.Y. Ma, E. Purba, K.J. Roberts, Z.P. Chen, E. Martin, J. Morris, R. Bytheway, An examination of the kinetics of the solution-mediated polymorphic phase transformation between α- and β-forms of L-glutamic acid as determined using online powder X-ray diffraction, Cryst. Growth Des. 8 (2008) 2205–2216.